

Observation of spin-glass behavior in nickel adsorbed few layer graphene

Sreemanta Mitra^{1,2,*}, Oindrila Mondal³, Sourish Banerjee², and Dipankar Chakravorty^{1,†}

¹ *MLS Prof.of Physics' Unit,
Indian Association for the Cultivation of Science,
Kolkata-700032, India.*

² *Department of Physics,
University of Calcutta,
Kolkata-700009, India.*

and

³ *Department of Physics,
M.U.C. Woman's College, Burdwan, India.*

Abstract

Nickel-adsorbed graphene was prepared by first synthesizing graphite oxide (GO) by modified Hummers' method and then reducing a solution containing both GO and Ni^{2+} . EDX analysis showed 31 atomic percent nickel was present. Magnetization measurements under both dc and ac magnetic fields were carried out in the temperature range 2 K to 300 K. The zero field cooled and field cooled magnetization data showed a pronounced irreversibility at a temperature around 20 K. The analysis of the ac susceptibility data were carried out by both Vogel-Fulcher as well as power law. From dynamic scaling analysis the microscopic flipping time $\tau_0 \sim 10^{-13}s$ and critical exponent $z\nu = 5.9 \pm 0.1$ were found, indicating presence of conventional spin glass in the system. The spin glass transition temperature was estimated as 19.5 K. Decay of thermoremanent magnetization (TRM) was explained by stretched exponential function with a value of the exponent as 0.6 . From the results it is concluded that nickel adsorbed graphene behaves like a spin-glass.

PACS numbers: 75.50.Lk, 75.78.-n, 76.60.Es

I. INTRODUCTION

Discovery of graphene has opened up many avenues of research because of basic physics and limitless possibilities of developing novel devices in the nanoscale, using this material.^{1,2} Not only are the electronic properties of unusual nature,^{3,4} the mechanical and thermal behaviour have also been found to be remarkable, the breaking strength and thermal conductivity exhibiting record values.⁵⁻⁷ Magnetism in graphene due to the presence of defects has been studied theoretically⁸ and recently observed experimentally.⁹ The edge state induced magnetism in graphene has also been observed both theoretically¹⁰ and experimentally.¹¹ Substitutional nickel impurities have been demonstrated to be present in graphenic carbon nanostructures, prepared by using nickel containing catalyst.^{12,13} Calculations based on spin density functional theory have indicated that substitutional nickel defects in flat graphene are non magnetic.¹⁴ A nonzero spin moment can however, be observed if the adsorbed nickel atoms lie along the edges of the graphene.¹⁵ We have synthesized nickel adsorbed graphene, starting from graphite oxide using a solution route. Detailed magnetization measurements under both dc and ac magnetic field were carried out. A spin-glass behaviour was observed. The details are reported in this article.

II. SYNTHESIS AND CHARACTERIZATION

Primarily, the graphite oxide (GO) was prepared from extra pure fine graphite powder (as obtained from LOBACHEMIE), using modified Hummers' method.^{16,17} The graphene oxide was prepared by stirring powdered flake graphite and sodium nitrate ($NaNO_3$), 2 g each and 6 g of potassium permanganate ($KMnO_4$) (98.5% pure, E Merck) into 50 ml concentrated sulfuric acid (98%, E-Merck). The ingredients were mixed in a beaker, that had been cooled to 273 K in an ice bath. The bath was then removed and the suspension brought to room temperature (300 K) and put under constant stirring for 2 h. As the reaction progressed, the mixture gradually thickened with a diminishing in effervescence. After 2 h, 300 ml water and 5 ml hydrogen peroxide (H_2O_2) were slowly added under stirring. The suspension was then filtered resulting in a yellow-brown filter cake. The filtrate was washed several times with 1:10 HCl solution in order to remove unwanted metal ions present.¹⁸ The collected washed sample was dried in an air oven at 333 K for 2 days.

Uniform aqueous dispersion of GO (0.01 g in 10 mL) was mixed with 10 mL 0.03 M solution of nickel nitrate (hexahydrate)($Ni(NO_3)_2 \cdot 6H_2O$) (E merck, Germany). The mixture was stirred thoroughly for 2 h. By adding ammonia solution to the mixture its pH was brought to a value ≈ 10 . 0.142 g sodium borohydride ($NaBH_4$) (0.37 M) was added to reduce GO and Ni^{2+} simultaneously to form Nickel adsorbed graphene. The sample was collected by centrifuging the aqueous mixture at 2000 rpm in an ultracentrifuge (elTek TC 4100D). The sample was then washed thoroughly with deionized water several times to remove any unreacted ions present. The sample was then dried at 348 K for 24 h.

The X-ray diffractogram was taken in a Bruker D8 SWAX diffractometer using Cu K_α monochromatic source of wavelength ($\lambda = 0.154$ nm). The microstructure was studied by using transmission electron microscope (JEOL 2010) operated at 200 kV. To study the chemical composition of the sample, Energy dispersive X-ray spectroscopy (EDX) was done using a JEOL JSM-6700F field-emission scanning electron microscope. Fourier transform infrared spectroscopy (FTIR) studies of the samples were carried out using FTIR8400S spectrometer. Both the dc and ac magnetic measurements were carried out by using a Superconducting Quantum Interference Device (SQUID) magnetometer (Quantum Design MPMS XL) with the reciprocating sample option (RSO) and a sensitivity of 10^{-7} emu. In order to obtain low magnetic fields the SQUID was demagnetized before the measurements.

III. RESULTS AND DISCUSSIONS

A. Structural Analysis

Figure 1(a) shows the x-ray diffractogram obtained from the nickel treated graphene. Only a hump around 25.6° is observed due to graphene.¹⁹ Since a monolayer graphene is not expected to show any diffraction peak, the small hump signifies that the system comprises few layer graphene. No signature of any diffraction peaks corresponding to either nickel or any of its oxides have been observed. The inset of figure 1(a) is the transmission electron micrograph of the nickel treated graphene. There is no evidence of any nanocluster being present in the micrograph. This is corroborated by the Figure 1(b) which shows the high resolution transmission electron micrograph (HRTEM) of the sample. The only interplanar spacing seen, has a value 0.3 nm which corresponds to the (002) reflection in graphene.¹⁹ In

the inset of figure 1(b) the electron diffraction pattern (SAED) obtained from figure 1(b) is shown. The absence of any diffraction spot also rules out the possibility of the presence of either Ni or NiO or Ni_3C in our system. The weak diffraction ring corresponds to plane (002) of graphene derived from GO. The absence of any other lattice plane means total absence of any nanoparticle in the system. It has, however, not been possible to characterize the position of the Ni atoms in graphene. Scanning tunneling microscopy (STM) could not be used because the sample is in powder form and therefore, it was difficult to mount in STM and pick up its position with reference to the graphene sheet. However, on the basis of the computational work reported in the literature^{15,20} we believe the nickel atoms to be forming bridgelike structure between two surface carbon atoms in graphene as shown schematically in figure 2. This is the equilibrium structure for the adatoms in graphene as shown theoretically.²¹ It is emphasized that these nickel atoms will have magnetic moments as opposed to the situation in which nickel atoms substitute carbon atoms in graphene layer.¹⁴

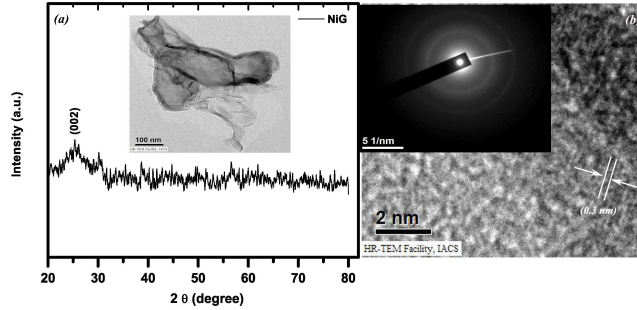


FIG. 1. (a) X-ray diffractogram of nickel treated graphene (b) Transmission electron micrograph of NIG. (c) SAED pattern obtained from (b). (d) HRTEM image of the sample.

B. Compositional Analysis

The FTIR spectra of graphite oxide (GO), chemically converted graphene (CCG) and nickel adsorbed graphene (NIG) have been shown in figure 3(a). The treatment of GO with $NaBH_4$ causes an enormous structural change (product CCG), which have been observed in FTIR spectrum. The spectrum for GO shows transmittance dips at 1390.65, 1634.23, and 1725.14 cm^{-1} , which correspond to deformation of O-H bond in water, stretching mode of carbon carbon double bond (C=C), and stretching mode of carbon oxygen double bond

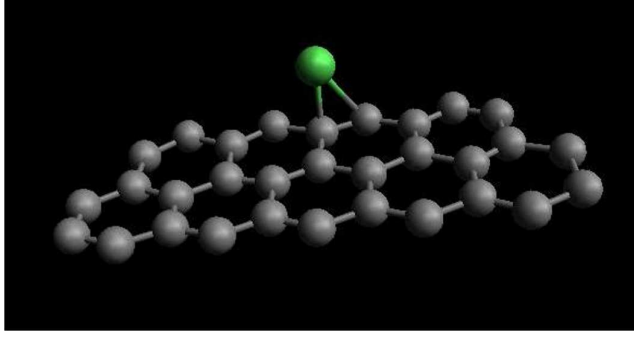


FIG. 2. Schematic representation of the nickel (green colored atom) adsorbed graphene system on the basis of computational work^{15,20}.

TABLE I. Elemental Analysis from EDX spectra of the specimen synthesized.

Element	Atomic %
Carbon	42.32
Nickel	19.07
Oxygen	38.61

(C=O), respectively. The broad dip at around 3400 cm^{-1} arises due to the bending of O-H bond in water¹⁹. It has been seen that there is no transmittance dip at around 1725 cm^{-1} , for CCG and NIG. So it is concluded that both CCG and NIG are free from oxygen functionality present in GO. Another extra transmittance dip (in comparison to CCG) around 2070 cm^{-1} (marked by red arrow) is observed for the NIG sample, which occurs due to the stretching mode of nickel carbon bond. In view of this unmistakable evidence, no other conclusion than that of the presence of C-Ni bond could be drawn. The formation of the Ni-C bond at the reaction condition used here is not surprising because of large surface to volume ratio in the graphene prepared which is therefore highly reactive. Figure 3(b) shows the EDX spectra of the system under study. From the EDX spectra it can be seen that no magnetic impurity, other than nickel, is present in the material.

The elemental analysis as obtained from the EDX data is shown in table 1. The amount of oxygen shown in table 1 comes from the H_2O molecules present in the system. It may be mentioned here that H can not be detected by the EDX. This has been made amply clear by earlier authors who prepared graphene by a similar method of chemically exfoliating GO.¹⁹ We have therefore, calculated the atomic percent of nickel after neglecting the amount of

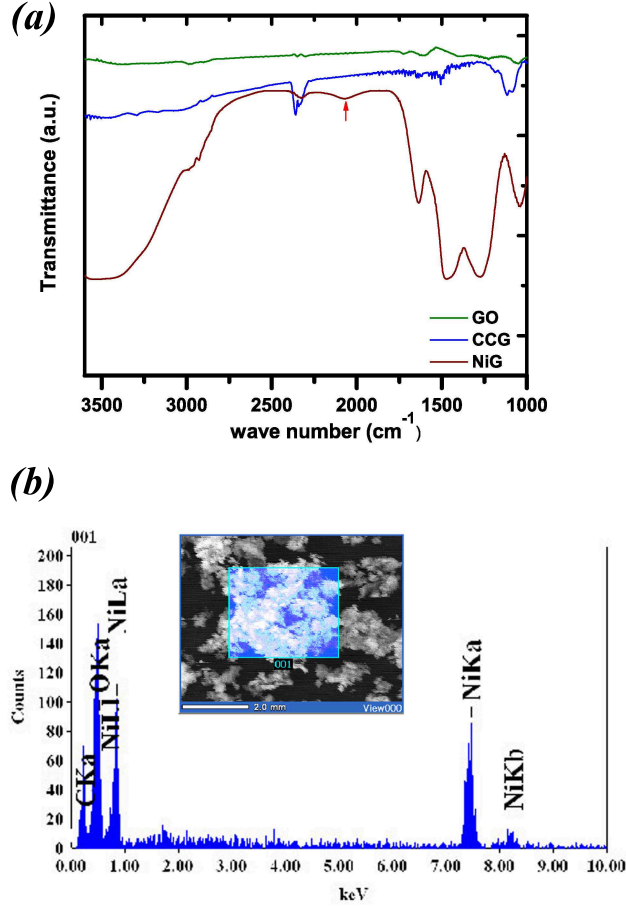


FIG. 3. (a)FTIR spectrograph of GO,CCG and NiG. (b) EDX spectra of the material under investigation.

oxygen shown in table 1 .

This suggests that 31 atomic % nickel is present in graphene network. It is to be noted that oxygen detected by EDX do not form any part of the graphene phase. From the selected area electron diffraction (SAED) image [figure 1(c)] it is concluded that neither nanoparticles of nickel nor any of its oxides have been formed. So, it can be safely concluded that nickel was adsorbed on the surface of the graphene,during the simultaneous reduction of GO and Ni^{2+} to graphene and atomic nickel respectively. This kind of structure has already been studied theoretically,^{14,15} which proves the stability of such structures.

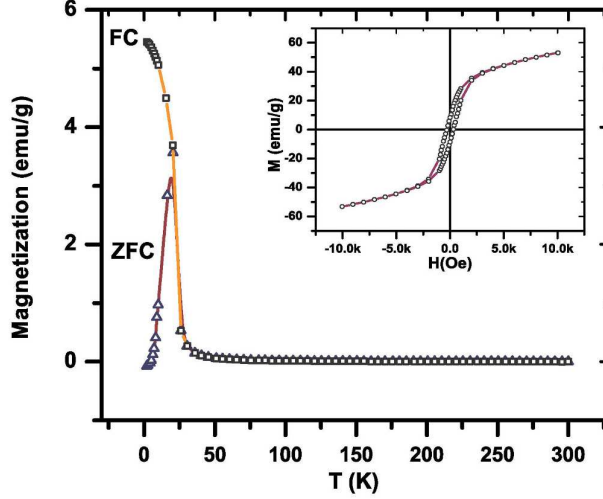


FIG. 4. The dc magnetization as measured in field-cooled (FC) and zero-field-cooled (ZFC) conditions at 100 Oe, exhibiting pronounced irreversibility at the freezing point. The inset shows the non-saturating M - H isotherm as measured at 10 K.

C. DC magnetization

For non-equilibrium systems, like spin glasses and superparamagnets, history effects in dc magnetization is a generic feature i.e. there is irreversibility in the data describing magnetization as a function of temperature. We observe a bifurcation in zero field cooled (ZFC) and field cooled (FC) curves in the magnetization-temperature data [figure 4] for the nickel adsorbed graphene. The data clearly show a pronounced irreversibility at $T \approx 20$ K. This shows the occurrence of magnetic history effect in the system. In the inset of figure 4, we have shown the M - H isotherm measured at 10 K indicating the presence of a finite coercivity. It is interesting to note that the deviation of the FC magnetization from the ZFC at the freezing point (temperature at which ZFC peak occurs) is a feature, however not exclusive, for the canonical spin glass system. This kind of behavior is also expected in the case of superparamagnets having narrow volume distribution. In both the cases of superparamagnets and spin glasses, finite dipolar interaction between the spins results in the deviation of FC -ZFC curves at temperatures lower than blocking or freezing temperatures and FC magnetization increases continuously as the temperature is lowered.²² It may be noted here that there have been recent reports on similar behavior of low temperature magnetization peaks obtained in nickel^{23,24} and nickel carbide^{25,26} nanoparticles respectively. We discuss

the implications as follows. In the case of nickel nanoparticles a peak is observed but the irreversibility in the magnetization/temperature behavior continues upto room temperature and above. This is the signature of superparamagnetism which is consistent with the fact that the systems show room temperature ferromagnetism. On the contrary, in our system, the irreversibility disappears after 20K. Also the value of the coercivity becomes zero, indicating that the system is in a paramagnetic state. Comparing the data of Ni_3C nanoparticles²⁵ with those of our own, we note, that in our case the magnetization value is two orders of magnitude higher. A robust ferromagnetism is observed below the freezing temperature rather than a weak ferromagnetism observed in the nickel carbide nanoparticle system.²⁵ We therefore, rule out the possibility of any Ni_3C nanoparticles being present in our sample. Also the peak in the ac susceptibility versus temperature plot was reported to be at $\sim 10K$, whereas, in our system it was found to be around 20K (see next section).

From the above discussion it follows that neither Ni nor Ni_3C nanoparticles are present in the system synthesized by us. Both the compositional analysis (previous section) and comparison of our magnetic data with carefully conducted magnetization studies on nano nickel and nano Ni_3C done earlier substantiate our description of the system under study to be nickel adsorbed graphene.

D. AC magnetization

In principle, the time dependent susceptibilities might give detailed insight into the dynamics of freezing. To probe the dynamics of the spin system, we measured the ac susceptibility of the sample at low magnetic field (0.5 Oe). The temperature dependence of the real (χ'_{ac}) and imaginary (χ''_{ac}) parts of the ac susceptibility of the present system are shown in figures 5(a) and 5(b) respectively for frequencies ranging from 10 Hz to 1kHz. It can be seen that the peak height in the ($\chi''_{ac} - T$) is increased and shifted towards high temperature side with the increasing frequency. It should be noted that for a conventional ferromagnet the imaginary part of the ac susceptibility vanishes above and below the peak temperature, but remains non-zero in case of a spin glass system.^{27,28}

In the case of a spin glass, both the real and imaginary parts of the ac susceptibility show a frequency dependent cusp or maximum at a temperature, called effective spin glass transition temperature $T_f(\omega)$, the value of which should increase with an increase in frequency.

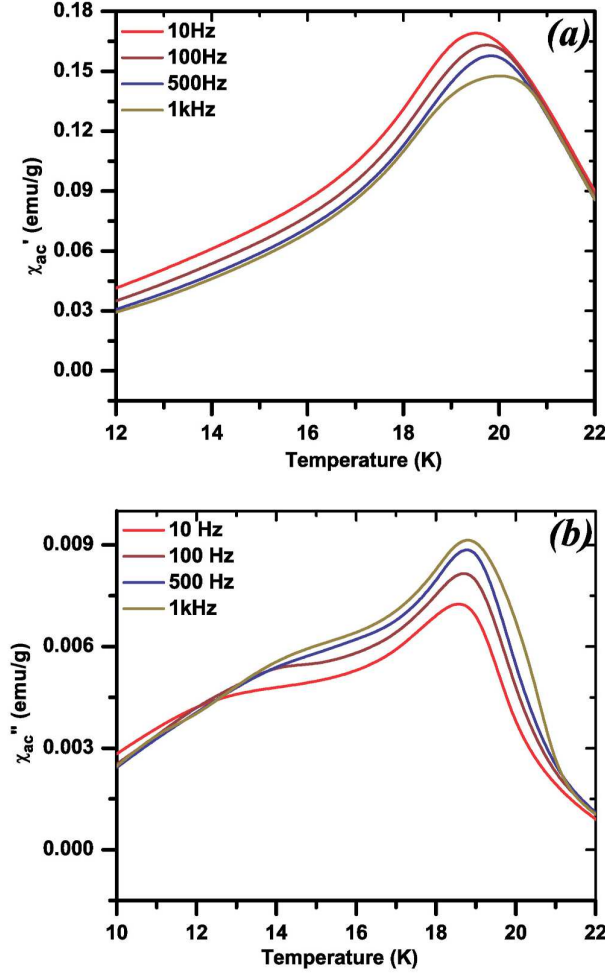


FIG. 5. The frequency dependence of the (a) real and (b) imaginary part of the linear susceptibility as measured at 0.5 Oe with the ac frequency being varied from 10 Hz to 1kHz.

We observe this particular behavior in our system as shown in figure 5. The frequency dependence of the peak temperature may be small, but this kind of small but clear dependance was previously observed in case of canonical spin glass systems.^{29,30} We have calculated the initial frequency shift of T_f from the frequency dependance of the peak temperature, by employing;^{31,32}

$$\delta T_f = \left[\frac{\Delta T_f}{T_f \Delta \log_{10} \omega} \right] \quad (1)$$

where, δT_f is the relative change in freezing temperature, ΔT_f is the total change in the T_f in the frequency interval, $\Delta \log_{10} \omega$ is the frequency interval. In our system δT_f comes out to be 0.01. For canonical spin glasses, the value of δT_f lies between 0.0045 to 0.06^{30,31,33} e.g. CuMn alloy shows a value of 0.005 and AuFe has the value 0.01³⁰. On the other hand

for known superparamagnets the value of δT_f is larger than 0.1.^{30,31} The ratio of the peak intensity of $Im(\chi_{ac})$ to $Re(\chi_{ac})$ is found to be 0.04, which is of the same order of magnitude as observed previously by Nishioka et.al.³⁴ on their study of canonical spin glass behavior in Ce_2AgIn_3 .

A widely used experimental technique, to measure the ‘characteristic time’ (τ), for describing the dynamical fluctuation time scale, is obtained from the observation time.^{27,35} The characteristic relaxation time of the spin system, at the in-phase susceptibility maximum corresponds to the observation time $t \sim \frac{1}{f}$.³⁶⁻³⁸

As this frequency dependent maximum of ac susceptibility is not a generic feature of spin-glass systems only, and can also be found for superparamagnets it is often difficult to distinguish between spin-glass and superparamagnetic behavior.^{27,30}

A non-interacting superparamagnetic cluster’s relaxation time follows the *Néel*-Arrhenius law^{36,39}

$$\tau = \tau_0 \exp\left(\frac{E_a}{k_B T_f}\right) \quad (2)$$

where E_a is the anisotropy energy barrier, k_B is the Boltzman constant, and T_f is the peak temperature. τ_0 depends on the gyromagnetic precession time and is usually of the order of $10^{-13} - 10^{-10}$ s. In our analysis $(\tau - T_f)$ data when fitted with equation (2) give values $\frac{E_a}{k_B} = 1250 \pm 320$ K and $\tau_0 \sim 10^{-30} (\ll 10^{-13})$ s. These are unphysical quantities and hence we conclude that observed susceptibility variation is not caused by the non-interacting superparamagnets.

In glassy systems, the strong temperature dependence of τ is frequently described by the law given by Vogel-Fulcher^{27,40,41}

$$\tau = \tau_0 \exp\left[\frac{E_a}{k_B(T_f - T_0)}\right] \quad (3)$$

where, the characteristic temperature, T_0 was introduced in an *ad-hoc* manner. The least square fitted results gave values $\frac{E_a}{k_B} = 11.93 \pm 0.56$ K, $T_0 = 18.92 \pm 0.03$ K with $\tau_0 = 9.35 \times 10^{-9}$ s. The value of τ_0 obtained for the system indicates the presence of conventional spin glass. A relatively larger value ($\sim 10^{-7}$ s) is expected for the interacting magnetic spin clusters.⁴² The data and the theoretically fitted curve have been shown in figure 6(a). It should be pointed out that in our system temperature dependence of the susceptibility maximum is small compared to a spin glass system reported earlier.⁴³ However, the nature of results is identical, the difference being a low value of the activation energy for spin flipping in our system. Using

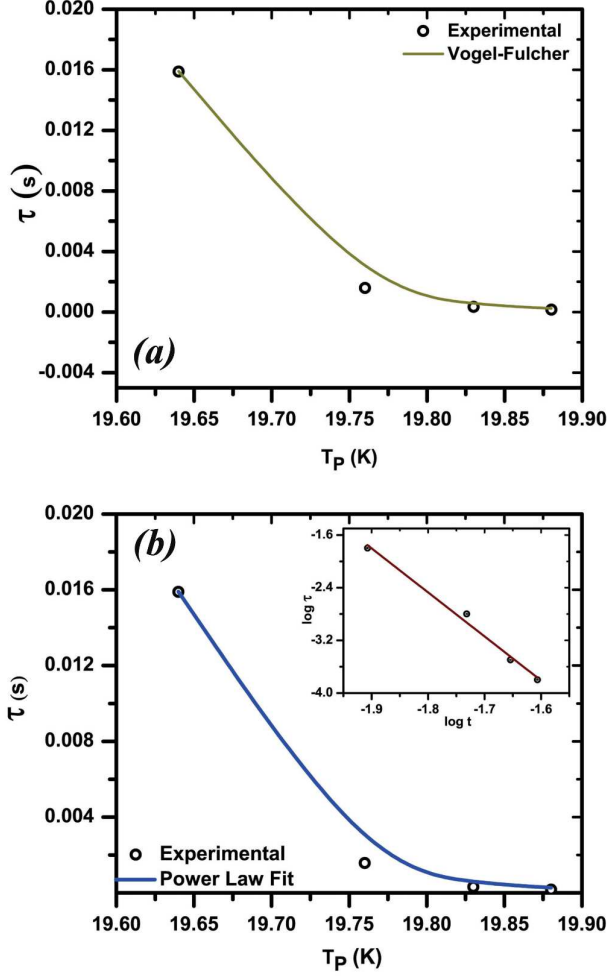


FIG. 6. The experimental variation of τ with peak temperature (T_P) and its fit with (a) Vogel-Fulcher Law and (b) Power Law. In the inset of (b) the variation of $\log \tau$ with logarithm of reduced temperature (t) shows a linear behaviour.

Vogel-Fulcher analysis, our results give $\frac{E_a}{k_B} = 11.93$ K whereas, Gunnarsson et.al.⁴³ results give $\frac{E_a}{k_B} = 56.2$ K. The value of T_0 suggests²⁷ that there is RKKY (Ruderman-Kittel-Kasuya-Yosida) type of interaction between the spins of atomic nickel, mediated via the highly conducting electrons of graphene, operative in our system. There are few theoretical works that describe that the RKKY interaction operative in graphene systems with adatoms on it, or having defects^{20,21,44,45} is short ranged because of low density of states of electrons near the Fermi level. However, in our method of sample preparation we obtained a few layers of graphene (FLG) as evidenced from the high resolution electron micrograph and x ray diffractogram [see section 3.1]. In the case of FLG systems the electronic structure will be

modified and there will be finite density of states at the Fermi energy.⁴⁶⁻⁴⁸ This will make the RKKY interaction between the atomic spins of nickel via the electrons of graphene quite feasible.

The sharp cusp in the temperature dependent ac susceptibility at low magnetic field indicates this to be a case of continuous phase transition. In case of a continuous phase transition, as the transition temperature is approached from above, the correlation length (ξ) diverges as $\frac{\xi}{a} = t^{-\nu}$ where, $t [= \frac{T_f - T_g}{T_g}]$ is the reduced temperature, with T_g as true glass transition temperature, T_f is freezing temperature, 'a' being the average distance between the interacting spins, ν is the critical exponent of the spin correlation length ξ . If the conventional critical slowing down while approaching T_g from higher T side is assumed, the relaxation time τ is related to ξ as $\tau \propto (\frac{\xi}{a})^z$, where, 'z' is the dynamic critical exponent. Thus the temperature dependence of the relaxation time τ can be expressed by a power law,^{27,49}

$$\tau = \tau_0 \left[\left(\frac{T_f}{T_g} \right) - 1 \right]^{-z\nu} \quad (4)$$

Figure 6(b) shows the fitting of the experimental data with the above mentioned power law, with τ_0 as the microscopic flipping time of the fluctuating entities. The comprehensive fitting gives $z\nu = 5.9 \pm 0.10$, $\tau_0 = 10^{-13}$ s. and $T_g = 19.5 \pm 0.02$ K. The inset of the figure 6(b) shows the variation of the relaxation time with reduced temperature (both in log scale) and the linear fit of the data. The linear fit also gave the same order of magnitude value of the parameters as previously obtained. The value of the critical exponent ($z\nu$) is characteristic of a spin glass system ($5 \leq z\nu \leq 11$)³⁰ and quite different from those characteristic of regular ferromagnets ($1.2 \leq z\nu \leq 2$).⁵⁰ It should be mentioned here that for all the analysis of the relaxation time, we have considered $\tau = (2\pi f)^{-1}$ and while deducing T_f the maximum of (χ'_{ac}) was used. Alternatively, the temperature derivative of real or imaginary parts of ac susceptibility could be used. In case of χ' or χ'' the prominent peak was observed at the same temperature, as expected, but in $(\chi''_{ac}-T)$ data we observe another hump at the lower temperature side which is surprisingly absent in $(\chi'_{ac}-T)$ data and it needs clarification. We have tried to analyse them with previously mentioned models, viz; Néel-Arrhenius; and Vogel-Fulcher; but none of them was able to explain their occurrence, giving unphysical values of the parameters with huge errors. However, the prominent peaks in the temperature dependence of the real and imaginary parts of the ac susceptibility in the light of a relaxation mechanism have been successfully analysed.

From the dynamical scaling analysis of the $(\tau-T)$ we found the microscopic flipping time to be of the order of 10^{-13} s, which is of the same order as that found in conventional spin glasses.⁴³ If it were a cluster like spin glass then the τ_0 value should have been of the order of 10^{-10} s as reported previously by different workers on their studies on different cluster like spin glass systems.^{35,51} This is quite easy to understand that the microscopic magnetic entities are atomic spins of nickel and not nanosized clusters of ferromagnetically coupled spins. The present analysis gives the value of the critical exponent $z\nu$ as 5.9, which is not only close to the theoretically predicted value for the short range Ising and Heisenberg spin glasses,⁵² but is also the experimentally observed value for well known conventional spin glass systems like CuMn alloy at 4.6 at.%.³⁶

From the analysis, it is evident that both the Vogel-Fulcher and the power law successfully explain the relaxation mechanism, with different sets of T_0 , T_g and τ_0 values. The difference between T_0 and T_g is quite small ($\sim 0.58K$), whereas, $(\tau_0)_{PL}$ differs from $(\tau_0)_{VF}$ by 4 orders of magnitude. This kind of different τ_0 values, using power law and Vogel-Fulcher law was previously obtained by Souletie and Tholence³⁶ from their study on different spin glasses.

We have determined the spin glass order parameter (q), starting from the susceptibility using the following equation²⁷

$$\chi(T) = \frac{C(T)[1 - q(T)]}{T - \theta(T)[1 - q(T)]} \quad (5)$$

where, both $C(T)$ and $\theta(T)$ are temperature independent constant in mean field theory, but varies slowly near the spin glass transition temperature. To evaluate $q(T)$, $[(\chi'_{ac})]^{-1}$ was extrapolated and from that $\theta(T_f)$ and $C(T_f)$ were estimated. Using Eq.(5) $q(T)$ was found to be⁵³

$$q(T) \approx \frac{1 - T\chi(T)}{[C(T_f) + \theta(T_f)\chi(T)]} \quad (6)$$

The values of $q(T)$ as derived by Eq.(6) is shown in figure 7. it is observed that the measured $q(T)$ decreases almost linearly with increasing temperature. The analysis of the data using $T_f = 19.48K$ shows a power law for $q(T)$, as predicted by the mean field theory.²⁷

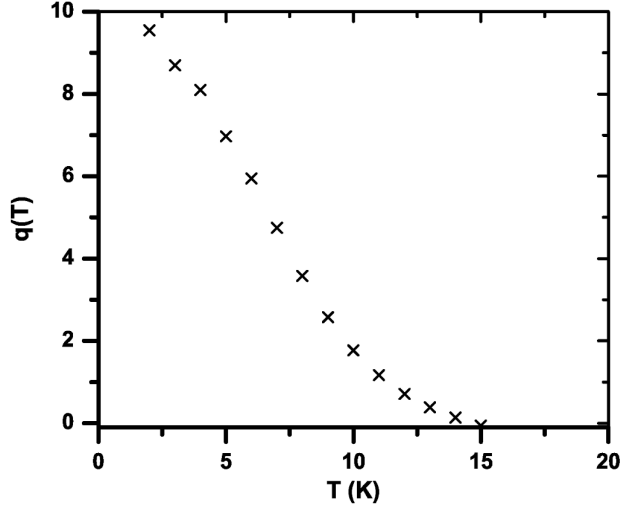


FIG. 7. Spin glass order parameter, $q(T)$, derived from the data of inverse susceptibility using Eq.(5).

E. Thermoremanent magnetization

One of the important characteristic features of spin-glasses is the phenomenon of aging. This occurs due to the breakdown of time translational invariance (as the magnetization evolves with time) of the response of the system under external perturbation. In spin glasses, a common way to explore aging is the decay of thermoremanent magnetization (M_{TRM}) with time. As the behavior of spin glass is complicated below freezing temperature due to ageing, we have taken an particular approach to measure the TRM relaxation. The TRM measurements were done at $0.72T_f$ (14 K) after cooling the sample under a magnetic field (10 Oe) from $2.0T_f$ (40 K). After stabilizing the temperature, the system was made to wait for a time t_w . Then the magnetic field was cutted off and the evolution of magnetization with time was recorded. Out of various functional forms, to describe the time variation of remanent magnetization for spin glass systems, we have adopted one of the most commonly used relations, viz; a stretched exponential function³⁵

$$M(t) = M_0 + M_r \exp\left[-\left(\frac{t}{\tau_r}\right)^\beta\right] \quad (7)$$

where, M_0 relates to an intrinsic ferromagnetic component, and M_r to a glassy component. the time constant τ_r depends on T and t_w , whereas, β is a function of T. For $\beta = 1$, the relaxation involves the activation against single energy barrier, and for $0 < \beta < 1$, it stands for SG systems; and $\beta = 0$ implies there is no relaxation at all. Our (TRM-T) data fitted

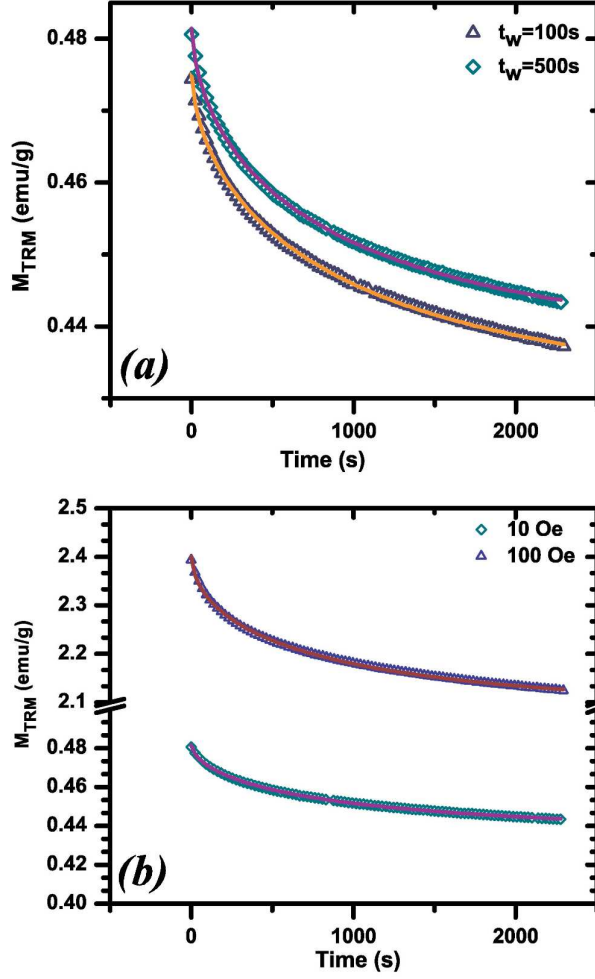


FIG. 8. (a) Time decay of M_{TRM} as measured at $0.72 T_f$ after cooling in the presence of a field of 10 Oe and for different wait times (t_w). (b) The variation of M_{TRM} with time for different magnetic field shown in a same graph. The solid lines are the theoretically fitted curves with the stretched exponential function [eq.7].

well with the above mentioned stretched exponential function, and did not follow the simple logarithmic decay. From the fitting the value of β was extracted as 0.61 ± 0.007 . Both the experimental and the theoretically fitted curves have been shown in figure 8. Figure 8(a) shows the evolution of thermoremanent magnetization for different wait times (viz; $t_w = 100s$ and $500s$) cooled under a magnetic field of 10 Oe. It is seen that the M_{TRM} evolved in identical manner, and relaxes more slowly for longer wait time. In figure 8(b) we presented the magnetic field dependence of $M(t)$. These showed that aging has an effect on the magnetic relaxation in the system under study as it was observed for different spin glass

like systems.^{33,54–58}

IV. CONCLUSIONS

In summary, we have synthesized nickel adsorbed graphene via simultaneous reduction of GO and nickel ions. The dc magnetization study along with frequency dependent ac magnetization and magnetic relaxation studies confirmed the spin glass like behavior in the system. The observed frequency dependence of the peak temperature in the ac susceptibility curve was successfully analysed by using both the Vogel-Fulcher and power law. The dynamic scaling analysis gave the values of the critical exponent $z\nu = 5.9 \pm 0.10$ and microscopic flipping time $\tau_0 \sim 10^{-13}s$. The value of τ_0 indicates the presence of conventional spin glass in the system under study. This nickel adsorbed graphene system has a true spin glass transition temperature $T_g = 19.4 \pm 0.02$ K as obtained from the dynamical scaling analysis. The thermoremanent magnetization decay was successfully explained by the stretched exponential function, giving the value of the exponent as 0.61 ± 0.007 . The value of the interaction parameter T_0 from Vogel-Fulcher analysis suggests an RKKY type of interaction between the atomic spins of nickel, where the interaction is mediated via the conducting electrons of graphenic carbon network.

ACKNOWLEDGEMENTS

Authors thankfully acknowledge the Department of Science and Technology, Govt. of India, New Delhi for support under an Indo-Australian Project on Nanocomposites. Sreemanta Mitra thanks University Grants Commission, New Delhi, India for awarding a Senior Research Fellowship. DC thanks Indian National Science Academy, New Delhi, India for an Honorary Scientist's position.

* sreemanta85@gmail.com

† mlsdc@iacs.res.in

¹ A. K. Geim and K. S. Novoselov, Nat. Mater. **6**, 183 (2007)

² A. K. Geim, Science **324**, 1530 (2009)

- ³ A. Becerril, J. Mao, Z. Liu, R. M. Stoltenberg, Z. Bao, and Y. Chen, ACS Nano **2**, 463 (2008)
- ⁴ K. Novoselov, A. Geim, S.V.Morozov, D.Jiang, M.I.Katsnelson, I.V.Grigorieva, S.V.Dubonos, and A.A.Firsov, Nature **438**, 197 (2005)
- ⁵ C. Lee, X. Wei, J. W. Kysar, and J. Hone, Science **321**, 385 (2008)
- ⁶ C. Gómez-Navarro, M. Burghard, and K. Kern, Nano Lett. **8**, 2045 (2008)
- ⁷ A. A. Balandin, S. Ghosh, W. Bao, I. Calizo, D. Teweldebrhan, F. Miao, and C. N. Lau, Nano Lett. **8**, 902 (2008)
- ⁸ H. Kumazaki and D. S. Hirashima, J.Phys.Soc.Jpn. **76**, 064713 (2007)
- ⁹ Y. Wang, Y. Huang, Y. Song, X. Zhang, Y. Ma, J. Liang, and Y. Chen, Nano Lett. **9**, 220 (2009)
- ¹⁰ H. Kumazaki and D. S. Hirashima, J.Phys.Soc.Jpn. **77**, 044705 (2008)
- ¹¹ S. K. Saha, M. Baskey, and D. Majumdar, Adv. Mater **22**, 5531 (2010)
- ¹² M. Ushiro, K. Uno, T. Fujikawa, Y. Sato, K. Tohji, F. Watari, W.-J. Chun, Y. Koike, and K. Asakura, Phys.Rev.B **73**, 144103 (2006)
- ¹³ F. Banhart, J.-C. Charlier, and P. M. Ajayan, Phys.Rev.Lett. **84**, 686 (2000)
- ¹⁴ E. J. G. Santos, A. Ayuela, S. B. Fagan, J. MendesFilho, D. L. Azevedo, A. G. SouzaFilho, and D. Sánchez-Portal, Phys.Rev.B **78**, 195420 (2008)
- ¹⁵ V. A. Rigo, T. B. Martins, A. J. R. da Silva, A. Fazzio, and R. H. Miwa, Phys.Rev.B **79**, 075435 (2009)
- ¹⁶ W. S. Hummers and R. E. Offeman, J. Am. Chem. Soc. **80**, 1339 (1958)
- ¹⁷ X. Zhou, X. Huang, X. Qi, S. Wu, C. Xue, F. Y. C. Boey, Q. Yan, P. Chen, and H. Zhang, J. Phys. Chem. C **113**, 10842 (2009)
- ¹⁸ N. I. Kovtyukhova, P. J. Ollivier, B. R. Martin, T. E. Mallouk, S. A. Chizhik, E. V. Buzaneva, and A. D. Gorchinskiy, Chem. Mater. **11**, 771 (1999)
- ¹⁹ K. S. Subrahmanyam, S. R. C. Vivekchand, A. Govindaraj, and C. N. R. Rao, J. Mater. Chem. **18**, 1517 (2008)
- ²⁰ Y. Mao, JianmeiYuan, and J. Zhong, J. Phys.:Cond. Mater. **20**, 115209 (2008)
- ²¹ P. O. Lehtinen, A. S. Foster, A. Ayuela, A. Krashenninnikov, K. Nordlund, and R. M. Nieminen, Phys.Rev.Lett. **91**, 017202 (2003)
- ²² W. Luo, S. R. Nagel, T. F. Rosenbaum, and R. E. Rosensweig, Phys.Rev.Lett. **67**, 2721 (1991)

- ²³ L. He, W. Zheng, W. Zhou, H. Du, C. Chen, and L. Guo, J. Phys.:Cond. Mater. **19**, 036216 (2007)
- ²⁴ W. Chen, W. Zhou, L. He, C. Chen, and L. Guo, J. Phys.:Cond. Mater. **22**, 126003 (2010)
- ²⁵ C. Chen, L. He, Y. Leng, and X. Li, J. Appl.Phys. **105**, 123923 (2009)
- ²⁶ L. He, J. Appl.Phys. **109**, 123915 (2011)
- ²⁷ K. Binder and A. Young, Rev.Mod.Phys. **58**, 801 (1986)
- ²⁸ A. A. Belik and E. Takayama-Muromachi, Inorg.Chem. **45**, 10224 (2006)
- ²⁹ F. Hellman, D. R. Queen, R. M. Potok, and B. L. Zink, Phys.Rev.Lett. **84**, 5411 (2000)
- ³⁰ J. A. Mydosh, *Spin Glasses: An Experimental Introduction* (Taylor and Francis, London,UK, 1993)
- ³¹ S. D. Tiwari and K. P. Rajeev, Phys.Rev.B **72**, 104433 (2005)
- ³² Y. T. Wang, H. Y. Bai, M. X. Pan, D. Q. Zhao, and W. H. Wang, Phys.Rev.B **74**, 064422 (2006)
- ³³ C. A. Cardoso, F. M. Araujo-Moreira, V. P. S. Awana, E. Takayama-Muromachi, O. F. de Lima, H. Yamauchi, and M. Karppinen, Phys.Rev.B **67**, 020407 (2003)
- ³⁴ T. Nishioka, Y. Tabata, T. Taniguchi, and Y. Miyako, J.Phys.Soc.Jpn. **69**, 1012 (2000)
- ³⁵ M. D. Mukadam, S. M. Yusuf, P. Sharma, S. K. Kulshreshtha, and G. K. Dey, Phys.Rev.B **72**, 174408 (2005)
- ³⁶ J. Souletie and J. L. Tholence, Phys.Rev.B **32**, 516 (1985)
- ³⁷ D. N. H. Nam, R. Mathieu, P. Nordblad, N. V. Khiem, and N. X. Phuc, Phys.Rev.B **62**, 8989 (2000)
- ³⁸ L. Sandlund, P. Granberg, L. Lundgren, P. Nordblad, P. Svedlindh, J. A. Cowen, and G. G. Kenning, Phys.Rev.B **40**, 869 (1989)
- ³⁹ L. Néel, Ann. Geophys. **5**, 99 (1949)
- ⁴⁰ H. Vogel, Phys. Z. **22**, 645 (1921)
- ⁴¹ G. S. Fulcher, J. Am. Ceram. Soc. **8**, 339 (1925)
- ⁴² C. Djurberg, P. Svedlindh, P. Nordblad, M. F. Hansen, F. Bødker, and S. Mørup, Phys. Rev. Lett. **79**, 5154 (1997)
- ⁴³ K. Gunnarsson, P. Svedlindh, P. Nordblad, L. Lundgren, H. Aruga, and A. Ito, Phys. Rev. Lett. **61**, 754 (1988)
- ⁴⁴ M. Sherafati and S. Satpathy, Phys.Rev.B **83**, 165425 (2011)

- ⁴⁵ M. Sherafati and S. Satpathy, Phys.Rev.B **84**, 125416 (2011)
- ⁴⁶ E. McCann and V. I. Falko, Phys.Rev. Lett. **96**, 086805 (2006)
- ⁴⁷ A. H. C. Neto, F. Guinea, N. M. R. Peres, K. S. Novoselov, and A. K. Geim, Rev. Mod. Phys. **81**, 109 (2009)
- ⁴⁸ B. A. McKinnon and T. C. Choy, Aust. J. Phys. **46**, 601 (1993)
- ⁴⁹ S. Nair and A. K. Nigam, Phys.Rev. B **75**, 214415 (2007)
- ⁵⁰ P. M. Chaikin and T. C. Lubensky, *Principles of condensed matter physics* (Cambridge University, Cambridge, England, 1995)
- ⁵¹ M.-H. Phan, T.-L. Phan, T.-N. Huynh, S.-C. Yu, J. R. Rhee, N. V. Khiem, and N. X. Phuc, J. Appl. Phys. **95**, 7531 (2004)
- ⁵² K. H. Fisher and J. A. Herz, *Spin Glasses* (Cambridge University, Cambridge, England, 1993)
- ⁵³ G. F. Zhou and H. Bakker, Phys.Rev. Lett. **72**, 2290 (1994)
- ⁵⁴ R. Mathieu, P. Jönsson, D. N. H. Nam, and P. Nordblad, Phys.Rev. B. **63**, 092401 (2001)
- ⁵⁵ M. Lederman, R. Orbach, J. M. Hammann, M. Ocio, and E. Vincent, Phys.Rev. B. **44**, 7403 (1991)
- ⁵⁶ R. V. Chamberlin, Phys.Rev. B. **30**, 5393 (1984)
- ⁵⁷ M. Alba, M. Ocio, and J. Hammann, Euro. Phys. Lett. **2**, 45 (1986)
- ⁵⁸ P. Nordblad, P. Svedlindh, L. Lundgren, and L. Sandlund, Phys.Rev. B. **33**, 645 (1986)